Design of Locally Enhanced Electric Field in Dielectric Loaded Rectangular Resonator for Quantum Microwave Measurements

Bo Wu[1], Yi Lin[1], Yi Liu[1], Qiang An[1], Dunwei Liao[1] and Yunqi Fu[1]

[1] *The College of Electronic Science and Technology, National University of Defense Technology, Changsha 410073, China*

Email: linyi_886@163.com

Rydberg-atom electrometers have the remarkable advantages of self-calibration and high sensitivity. Based on the classical electromagnetic theory, a localized electric field enhancement structure of a hybrid rectangular resonator is proposed to improve the sensitivity of quantum microwave measurement. It should be noted that the prototype of the hybrid rectangular resonator is fabricated and measured at 9.925 GHz. The results of full-wave simulations show that the uniform and high electric field enhancement in the TE101 fundamental mode is realized. The transient process of resonance is simultaneously simulated, and the time to settle steady state is given as about 104 ns. As indicated through experimental results that the structure can reach 24 dB (enhancement factor of 15.8). As a result, the method proposed in this study, based on atomic measurement capabilities, enables us to improve the measurement sensitivity further and promotes the practical development of quantum microwave measurement technology.

Introduction. With the rapid increase in demand for microwave applications, classical microwave technology faces many challenges. For instance, the size of the microwave terminal equipment is strictly limited by the Chu limit [1]. Furthermore, we must calibrate such probes to obtain accurate measurement values [2]. Hence considering the shortcomings above, quantum microwave measurement technology is a better alternative [3-4]. In the past five years, researchers have theoretically demonstrated that a sensitivity limit is as high as ten pV/cm/Hz$^{1/2}$[5], far exceeding the classical receiver sensitivity limit of -174 dBm/Hz (room temperature). Meanwhile, scholars have put forward solutions for improving the experimental measurement value of sensitivity. Mingyong Jing used the spatial superheterodyne method to increase the sensitivity to 55 nV/cm/Hz$^{1/2}$[6]. However, the sensitivity measurement capability has currently not reached the level of classical receivers. Studies are ongoing with classical electromagnetic theory to improve the sensitivity based on existing quantum measurement capabilities. Holloway's team has proposed a split plate resonator embedded in a vapor cell [7], amplifying the incident electric field strength in a small space. The electric field strength is amplified by 16.2 times (24 dB), but the fabrication of this structure is slightly complicated. On this basis, the team has proposed a split-ring resonator structure to achieve resonance enhancement of the incident microwave electric field [8]. However, these works don't mention the method of homogeneity electric field and the time-domain process of reaching the steady state.

In this paper, based on traditional electromagnetic theory, a localized electric field enhancement structure of a hybrid rectangular resonator (rectangular resonator, RR) is proposed to improve the electric field strength of the laser beam path in the cesium vapor cell. The experimental results verify the local enhancement ability of the structure to the electric field.

Design of the hybrid rectangular resonator. Here, the sensor consists of RR structures connected with two dielectric walls in the manner of a two-layer construction and a cesium atomic vapor cell, as illustrated in Fig. 1(a). The measured prototype geometry can be briefly described in Fig. 1(b).

In order to make the electric field strength of the TE101 mode more uniform, the relationship between the dielectric constant and the thickness of the dielectric walls is studied in this paper. The rectangular cavity's resonant frequency f_0 can be calculated roughly by[9]

$$f_0 = \frac{d_2 + 2d_4}{2\pi}\sqrt{\left(\frac{d_1}{\pi}\right)^2 + \left(\frac{d_3}{\pi}\right)^2} \tag{1}$$

According to dyadic Green's function [22], the TE101 fundamental mode in the x-direction can be expressed as

$$\nabla \times (\sin(\frac{\pi}{d_1})g(x)\vec{x}) \tag{2}$$

in which $g(x)$ satisfies wave equation and boundary conditions ignoring side openings:

$$\begin{cases} \dfrac{\mathrm{d}^2 g_{1,3}(x)}{\mathrm{d}x^2} + \left(\varepsilon_r\lambda^2 - \left(\dfrac{\pi}{d_1}\right)^2\right)g_{1,3}(x) = 0, \\ 0 \text{"} x < d_4, d_2 + d_4 \text{"} x < d_2 + 2d_4 \\ \dfrac{\mathrm{d}^2 g_2(x)}{\mathrm{d}x^2} + \left(\lambda^2 - \left(\dfrac{\pi}{d_1}\right)^2\right)g_2(x) = 0, \\ d_4 \text{"} x < d_2 + d_4 \end{cases} \tag{3}$$

$$\begin{cases} g_1(0) = 0, g_3(d_2 + 2d_4) = 0 \\ g_1(d_4) = g_2(d_4), g_2(d_2 + d_4) = g_3(d_2 + d_4) \\ g_1'(d_4) = g_2'(d_4), g_2'(d_2 + d_4) = g_3'(d_2 + d_4) \end{cases} \tag{4}$$

From equations (2)-(6), the $g_{1,2,3}(x)$ can be expressed as

$$\begin{cases} g_{1,3}(x) = C_{1,2}\sin\sqrt{\varepsilon_r\lambda^2 - \left(\frac{\pi}{d_1}\right)^2}\,x + C_{3,4}\cos\sqrt{\varepsilon_r\lambda^2 - \left(\frac{\pi}{d_1}\right)^2}\,x \\ g_2(x) = C_5\sin\sqrt{\lambda^2 - \left(\frac{\pi}{d_1}\right)^2}\,x + C_6\cos\sqrt{\lambda^2 - \left(\frac{\pi}{d_1}\right)^2}\,x \end{cases} \tag{5}$$

where C_{1-6} is constant, ε_r is permittivity.

When $\lambda = \frac{\pi}{d_1}$, $\cos\sqrt{\lambda^2 - \left(\frac{\pi}{d_1}\right)^2}\,x = 1$, $g_2(x) = C_6$ .When $\sqrt{\varepsilon_r\left(\frac{\pi}{d_1}\right)^2 - \left(\frac{\pi}{d_1}\right)^2}\,d_4 = \frac{\pi}{2}, g_{1,3}(x) = C_{1,2}$.*So,* $d_4 = \frac{d_1}{2\sqrt{\varepsilon_r - 1}}$.

At this point, we can obtain the condition of uniform field inside TE101.Based on the above analysis, the design parameters of Fig. 1 and Fig. 2 can be obtained easily.

Result. To find the resonant frequency of the set fundamental mode TE101, we measure the resonant microwave electric field mode reflection coefficients in Fig. 3. Then, transient analysis in Fig. 4 and electric field distribution in Fig. 5 of the RR are analyzed. The vector network analyzer measures that the fundamental mode

TE101 of RR resonant frequency is 9.925 GHz. The coaxial connector causes the resonance point at 10.075 GHz.

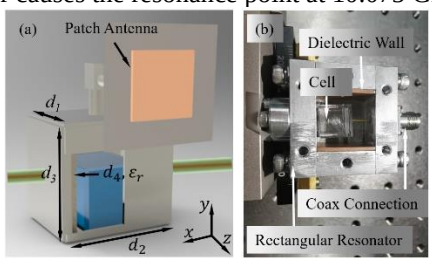

Fig. 1. *The perspective and geometrical details of the proposed RR are presented as its specific geometry parameters. (a)Simulation model. (b)Measured prototype. (d1=14 mm, d2=18.5 mm, d3=17 mm, d4=1.13 mm, d5=10 mm, ε_r=47.) All the thickness of metal is aluminum 7 mm.*

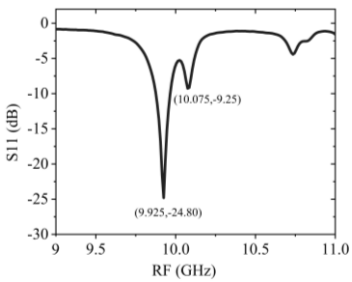

Fig. 2. *Measured reflection coefficient of the RR.*

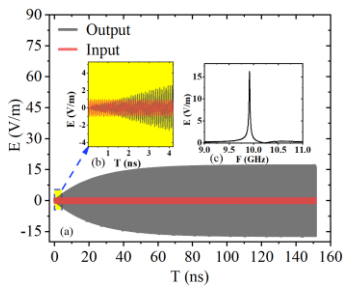

Fig. 3. *Simulated transient analysis of microwave electric field strength. (a) The partially enlarged insert shows the curve of the electric field versus the time. The red curve corresponds to the incident single-frequency continuous wave, and the gray curve corresponds to the electric field probe response to the incident wave. (b) This figure presents electric field versus frequency curve. (c) This figure illustrates electric field versus time curve. The purple dot corresponds to the steady-state.*

For signal modulation, the time for the RR resonance to settle to a steady-state is critical. Fig. 4 shows the simulated transient analysis results of microwave electric field strength. In this time-dependent incident electric field response curve, the electric field probe is set at the center of the cavity. The input signal is a 9.925 GHz single-frequency continuous wave with an electric field strength of 1 V/m. The output signal reaches a steady state at 104 ns. In the frequency domain analysis, the electric field strength is 16.3 V/m in Fig. 4(c), corresponding to an electric enhancement factor of 16.3 at 9.925 GHz.

To determine the homogeneity of the TE101 resonant field mode, we compare the three situations of 2D electric field distribution in Fig. 5(a)-(c). The situation where RR electric field local enhancement structure is loaded with the dielectric walls is better than that without dielectric walls. From the perspective of a one-dimensional cumulative distribution histogram generated at the same resonant frequency by sampling a cylinder region of about a million samples in Fig. 5(d), the slopes(K) when the electric field is 0.35 are 1.018 and 0.882, respectively. The diameter of 1 mm and the length of 10mm correspond to the probe laser and coupling laser beam size. The RR electric field local enhancement structure with dielectric walls and holes has a more uniform electric field distribution than that without dielectric walls.

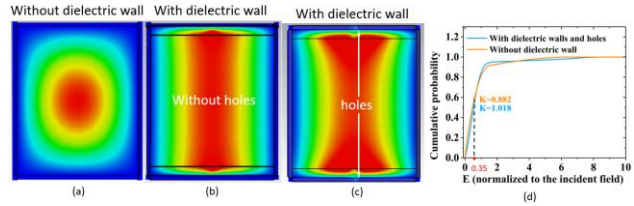

Fig. 4. *(a)-(c) These figures show comparison between simulation of TE101 resonant mode 2D electric field distribution in the RR for no dielectric wall and no hole, with dielectric walls and no hole, with dielectric walls and hole respectively. (d)This figure presents a cumulative histogram of the normalized electric field within the beam. The orange curve corresponds to without dielectric walls, and the blue curve corresponds to with dielectric walls and holes.*

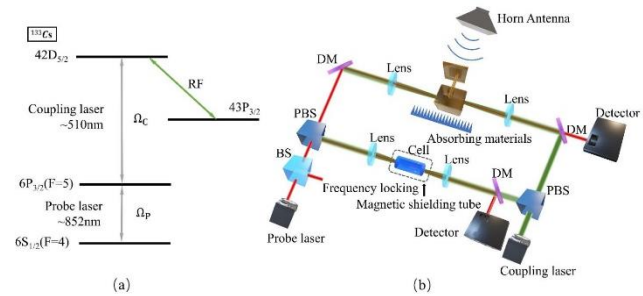

Fig. 5. *(a)Atomic levels used in the EIT scheme. States 6S1/2(F=4),6P3/2(F=5), and Rydberg state 42D5/2 are resonantly coupled by a probe laser (Ω_P) and coupling laser (Ω_C), respectively. A microwave electric field(green) is resonant with Rydberg transition 42D5/2 →43P3/2. (b) Overview of the experimental setup. We have also used the following notations: (1) DM: dichroic mirror, (2) PBS: polarizing beam splitter, and (3) BS: beam splitter*

Discussion. Atomic levels are shown in Fig. 5(a). The cesium atom is used as the excited atom. The probe laser of wavelength 852 nm drives the transition from the atomic ground state 6S1/2(F=4) to an intermediate state 6P3/2(F=5) with Rabi frequency Ω_P . An intense coupling laser of wavelength 510 nm acts on the transition between state 6P3/2(F=5) and Rydberg state 42D5/2 with Rabi frequency Ωc. The 9.925 GHz microwave field is used to couple transition for the states 42D5/2 → 43P3/2. The experimental setup for the RR electric field local enhancement structure experiment is shown in Fig. 5(b). A cubic vapor cell containing cesium atoms with a side length of 10mm is used. Probe laser and coupling laser are counter-propagating and overlapped through the center of the vapor cell within RR. The probe laser frequency is locked at the resonance frequency of 6S1/2(F=4) →6P3/2(F=5). At the same time, the coupling laser is scanned around the resonance frequency of 6P3/2(F=5) →42D5/2 coupling laser. The absorption of probe laser is detected by the detector, converting the optical signal into an electrical signal, and leading it to the detector to obtain the EIT spectrum at room temperature. In this way, the response of the Rydberg atoms to the applied

electromagnetic field can be directly reflected on the detector by the change of the probe laser strength. The EIT signal in the magnetic shielding tube is used as the reference signal. The microwave field is generated by a signal generator (SIG) with a maximum output power of 19 dBm and is emitted by a standard horn antenna operating at 2-18 GHz. The antenna is placed 30 cm in front of the vapor cell, and the polarization is co-linear with two lasers. The electric field at 9.929 GHz can take a couple of resonantly to the transition of 42D5/2→43P3/2. The loss of right-angle SMA is 0.4 dB, and the gain of the patch antenna is 7.6 dB in 9.925 GHz.

At room temperature, the intense coupling laser and the weak probe laser act together on the cesium atoms, which reduces the absorption of the probe laser by the cesium atoms, resulting in the EIT effect. The transmission peak of the probe laser can be obtained on the EIT spectrum, as shown in Fig. 6(a). On this basis, the near-resonant transition of 42D5/2→43P3/2 is driven by a detuning of the microwave electric field of 9.925 GHz. The absorption of the probe light is subjected to constructive interference, resulting in AT splitting, and the EIT transmission peak is split into two transmission peaks, obtaining the EIT-AT spectrum, as shown in Fig. 6(b). The AT splitting is proportional to the electric field strength $|E|$ and is perceived as [10]

$$|E| = \Omega_M = \frac{2\pi\hbar}{\wp_{MW}}\Delta f \tag{9}$$

where Ω_M is the Rabi frequency of the Rydberg state transition, $\wp_{MW}$ is the transition dipole moment of the adjacent Rydberg states, and $\hbar$ is Planck's constant. For cesium atom 42D5/2 →43P3/2 dipole element $\wp_{MW}$=1337 $a_0 e$, where a_0 is Bohr radius and e is electric charge. When near-resonant occurs, the relation between Rabi frequency Ω_M and detuning frequency Δf can be given by

$$\Delta f = \sqrt{{\Delta_M}^2 + {\Delta f_0}^2} \tag{7}$$

where Δf is the dependence of the splitting interval in Fig.7; detuning frequency is $\Delta_M = f - f_0$, f is the measured 9.925 GHz electric field, and f_0 is the resonance frequency the transition of 42D5/2→43P3/2 9.929 GHz. Here f_0 is the splitting interval induced by the resonant microwave electric.

Fig. 7(b) shows the asymmetric height of the splitting peaks under the detuning frequency 4 MHz Δ_M is 4 MHz and Δf is 4.856 MHz.According to equation (6)-(7), the detectable electric field strength $|E_1| = 0.0227$ V/m. The SIG feeds a near-resonant signal of 9.925 GHz, -22 dBm with RR corresponding to the red curve and 2 dBm without RR corresponding to gray curve. Note that the red and the gray curve have the same AT splitting. In addition, without the RR, no AT splitting is spotted in the EIT signal for -22 dBm. It can be observed that the same AT splitting (corresponding to the same detectable electric field strength) can be obtained by attenuating the SIG by 24 dBm after loading the RR local enhancement structure. Thus, the RR electric field local enhancement structure provides an electric field enhancement factor of 15.8($10^{24/20} = 15.8$). This proves that the quantum sensor with the RR electric field local can detect an electric field 15.8 times weaker than that without the RR. The main differences between the experimental test results (24 dB) and the simulation results (24.3 dB) are the machining error and test error.

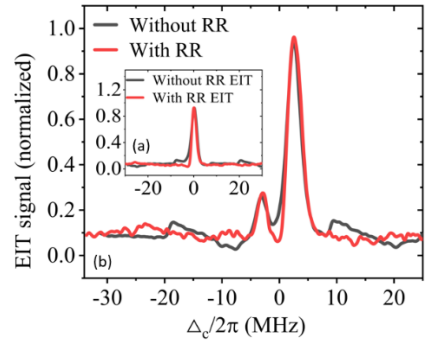

Fig. 7. *(a)The insert shows experimental data for the EIT transmission signal. (b)Red curve and gray curve present AT splitting with RR for a SIG power of -22 dBm and without RR for a SIG power of 2 dBm, respectively.*

Conclusion: In this paper, we propose a hybrid RR electric field local enhancement structure that integrates the characteristics of the high electric field, the homogeneity performance, and a straightforward design. We have demonstrated the feasibility of the scheme of hybrid RR electric field local enhancement structure by both simulation and experiment. The transient process of resonance is simulated, and the time to settle steady state is given as about 104 ns. The measured results show that RR's electric field enhancement factor is 15.8 times. Encouragingly, the approach is expected to effectively increase the sensitivities and be applied to the wireless receiver system.

References

1. Chu, Lan Jen. "Physical limitations of omni-directional antennas." Journal of applied physics 19.12 (1948): 1163-1175.
2. 2011 Holloway, Christopher L., et al. "Broadband Rydberg atom-based electric-field probe for SI-traceable, selfcalibrated measurements." IEEE Transactions on Antennas and Propagation 62.12 (2014): 6169-6182.
3. Yan-Li Zhou, Dong Yan, and Weibin Li, Rydberg electromagnetically induced transparency and absorption of strontium triplet states in a weak microwave field, Phys. Rev. A 105, 053714 (2022).
4. Yang K, Sun Z, Mao R, et al. A wideband Rydberg atom-based receiver for AM radio frequency communication[J]. Chinese Optics Letters Vol. 20, Issue 8, (2022)
5. Meyer D H , O'Brien C , Fahey D P , et al. Optimal Atomic Quantum Sensing using EIT Readout[J]. 2021.
6. Jing M, Hu Y, Ma J, et al. Atomic superheterodyne receiver based on microwave-dressed Rydberg spectroscopy[J]. Nature Physics, 2020, 16(9): 911-915.
7. Anderson D A , Paradis E G , Raithel G . A vapor-cell atomic sensor for radio-frequency field detection using a polarization-selective field enhancement resonator[J]. Applied Physics Letters, 2018, 113(7):073501.1-073501.5.
8. Anderson D A , Raithel G A , Paradis E G , et al. Atom-Based Electromagnetic Field Sensing Element and Measurement System, US10823775B2[P]. 2019.
9. Tai, Chen-To, and G. Eleftheriades. "Dyadic green functions in electromagnetic theory." IEEE Proceedings. Vol. 83. No. 6. [New York, NY]: Institute of Electrical and Electronics Engineers,[1963-, 1995.
10. Zhang L, Jia Y, Jing M, et al. Detuning radio-frequency electrometry using Rydberg atoms in a room-temperature vapor cell[J]. Laser Physics, 2019, 29(3): 035701.